Directional off-Normal Photon Streaming from Hybrid Plasmon-Emitter Coupled Metasurfaces

Kan, Yinhui; Ding, Fei; Zhao, Changying; Bozhevolnyi, Sergey I.

Published in:
ACS Photonics

DOI:
10.1021/acsphotonics.0c00196

Publication date:
2020

Document version:
Accepted manuscript

Citation for pulished version (APA):
Kan, Y., Ding, F., Zhao, C., & Bozhevolnyi, S. I. (2020). Directional off-Normal Photon Streaming from Hybrid Plasmon-Emitter Coupled Metasurfaces. *ACS Photonics*, *7*(5), 1111-1116.
https://doi.org/10.1021/acsphotonics.0c00196

Directional off-normal photon streaming from hybrid plasmon-emitter coupled metasurfaces

Journal:	*ACS Photonics*
Manuscript ID	ph-2020-00196d.R1
Manuscript Type:	Letter
Date Submitted by the Author:	26-Mar-2020
Complete List of Authors:	Kan, Yinhui; Shanghai Jiao Tong University School of Mechanical Engineering; University of Southern Denmark, Center for Nano Optics Ding, Fei; Syddansk Universitet, Department of Technology and Innovation Zhao, Changying; Shanghai Jiao Tong University, School of Mechanical Engineering Bozhevolnyi, Sergey; University of Southern Denmark, Centre for Nano Optics

Directional off-normal photon streaming from hybrid plasmon-emitter coupled metasurfaces

Yinhui Kan[1,2], Fei Ding[2], Changying Zhao[1], Sergey I. Bozhevolnyi[2]**

[1]Institute of Engineering Thermophysics, Shanghai Jiao Tong University, Shanghai, 200240, China

[2]Center for Nano Optics, University of Southern Denmark, DK-5230 Odense M, Denmark

ABSTRACT: Efficiently funneling photon streams from quantum emitters (QEs) in controllable directions is essential for interfacing the photon emission from nanoscale volumes with complex optical configurations exploited in quantum information and communication systems. We propose hybrid plasmon-QE coupled metasurfaces featuring circular nanoridges with displaced centers to funnel the photon emission along a given off-normal direction. The design principle relies on phase matching QE-excited circularly diverging surface plasmons to a well-collimated off-normal propagating photon stream by using a modified bullseye antenna with circular nanoridges having appropriately displaced centers. We demonstrate with the simulations that the hybrid plasmon-QE coupled metasurfaces enable highly directional off-normal photon emission with collection efficiencies exceeding 96%. Using nanodiamonds with multiple nitrogen vacancy centers, we experimentally demonstrate the directional photon streaming with different, up to 17.3°, off-normal angles and efficiencies reaching 90% for solid angles of < 0.1 sr.

KEYWORDS: quantum emitter, plasmonics, unidirectional emission, collection efficiency, fluorescence

Efficient collection of photons radiated by quantum emitters (QEs) is crucial for many quantum technologies, including quantum entanglement,[1-3] quantum computation,[4,5] and sensing.[6-8] Typical unmodified QEs, such as molecules,[9,10] quantum dots,[11-13] and defects in diamonds,[14-16] feature electric-dipolar emission patterns with poor directionality, thus resulting in relatively low collection efficiencies that would hinder QEs being directly used in practical applications. To realize the QE directional emission, one would resort to either geometrical (far-field) or near-field beam-shaping approaches. The geometrical approaches typically involve redirecting and reshaping of the far-field QE emission by its focusing, reflecting, and refracting with mirrors and lenses, thereby unavoidably reducing the collection efficiency and requiring the use of bulky optical components.[17-19] Alternatively, the near-field coupling approaches rely on the non-radiative QE interaction with surrounding nanostructures, thus enabling a direct and efficient control of the far-field QE emission with highly compact configurations.[20-23]

In recent years, QE coupling to nanoantennas/nanocavities has emerged as one of the most rapidly growing research topics in nano-optics.[24-33] Nano-patch antennas have been demonstrated to enhance the spontaneous emission rate (the so-called Purcell effect), while also modifying and, to some extent, improving the QE emission directivity.[28,29] Yagi-Uda antennas have been found useful for funneling the QE emission into a specific direction by placing a QE near the feed element.[30-33] However, the resulting emission is not well collimated, featuring a relatively large angular dispersion and thus resulting in a relatively low collection efficiency. QE-coupled bullseye gratings formed by periodic concentric rings were introduced for improving the collection efficiency. Different kinds of bullseye gratings have been proposed, including bullseye apertures in metal films, metal bullseye

structures, and hybrid plasmonic bullseye antennas.[21,22,34-37] Among them, the hybrid plasmonic bullseye antennas, composed of dielectric nanoridges on metal substrates with dielectric spacers, appear most attractive from the viewpoint of combining high quantum yield and collection efficiency.[22] At the same time, the QE emission is concentrated around the normal to the sample surface due to the bullseye symmetry, limiting the design flexibility with respect to the control over the QE emission direction, which is in turn highly desired in quantum optics and nanophotonics.

Here, we propose and demonstrate hybrid plasmon-QE coupled metasurfaces based on a modified bullseye antenna with circular nanoridges having appropriately displaced centers, a configuration that facilitates the phase matching of QE-excited circularly-diverging surface plasmon polaritons (SPPs) and a well-collimated off-normal propagating photon stream. First, the design principle is introduced with qualitative considerations and supported with numerical simulations. In the subsequent experiments, we assemble the hybrid plasmon-QE coupled metasurfaces by using nanodiamonds (NDs) containing nitrogen vacancy centers (NV centers) as QEs, which are surrounded by precisely positioned dielectric bullseye-displaced antennas. The experimental results are in excellent agreement with numerical simulations, demonstrating highly directional off-normal photon emission with high collection efficiencies.

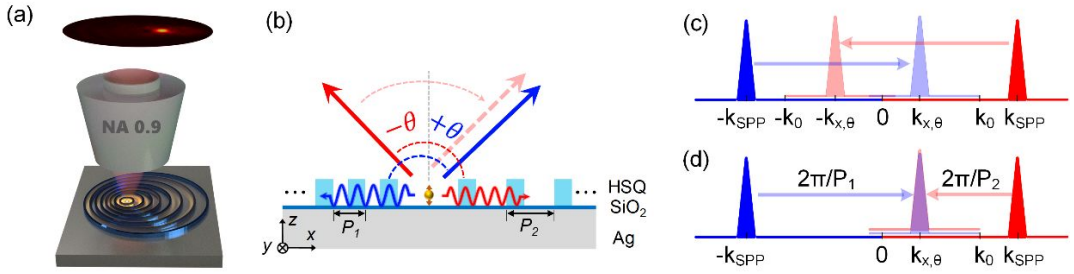

Figure 1. (a) Schematic of unidirectional and off-axis emission from a hybrid plasmonic-QE coupled system. (b) The cross-section view of the system. The gratings with different periods on two sides can unidirectionally outcouple the counterpropagating SPPs into oblique angles. (c) Schematic of the

symmetric unidirectional outcoupling in the wave vector domain, resulting in two outcoupled waves propagating under different angles. Red and blue peaks represent respectively the right- and left-propagating SPP waves. Arrows indicate the coupling direction. (d) Schematic of the synchronized asymmetric outcoupling that results in as single wave propagating under an oblique angle.

The schematic and operation principle of the plasmon-QE coupled system are shown in Figure 1. A QE, situated in the center of the inner ring, is adjacent to the metal substrate to spontaneously decay through the excitation of SPPs propagating along the dielectric-metal interface. SPPs are scattered and subsequently converted into a stream of free-space light by the bullseye-like Doppler nanoridges with different periods on two sides, resulting in unidirectional off-axis emission. Figure 1b shows the cross-section of the structure, which is composed of the Hydrogen silsesquioxane (HSQ) bullseye-like Doppler gratings on top of a silica covered silver film. The 20-nm-thin silica spacer layer used here can not only mitigate the quenching of QEs but also protect silver from being oxidized. The SPPs excitation would dominate the decay channel beyond photon radiation or nonradiative metal quenching when the dipole and metal surface are separated slightly larger than ~10 nm, ensured here by the silica spacer layer. The HSQ bullseye-like gratings have the ridge height H = 150 nm and two different periods in the x direction, i.e., P_1 and P_2 satisfying $P_1 = P - \Delta$ and $P_2 = P + \Delta$, where P is the default period that equals to the effective wavelength λ_{eff} of the SPPs, and Δ is the displacement between centers of two neighbor circular ridges. This is a simplified design that allows one to employ circular ridges having the same radii in all configurations (used for the SPP out coupling at different sloping angles), with the only adjustment being that the neighbor circles are displaced (along the x-axis) in accordance with the targeted outcoupling angle (see Supporting Information, section 1). Along the y-direction, there is no displacement, the ridges remain concentric, and the SPP scattering into free-space propagating waves is symmetric, as shown in Figure 1c, due to the identical periods on two sides and thereby equal transverse wavevectors of the outcoupled

propagating waves. Along the *x*-direction, due to the displacement between centers of two neighbor circular ridges, different periods on two sides would provide different reciprocal vectors (i.e., $2\pi/P_1$ and $2\pi/P_2$), and the SPP scattering into free-space propagating waves becomes asymmetric, as shown in Figure 1c, which results in a sloping angle for the outcoupled propagating waves. With properly designing the periods of the gratings on two sides, it is possible to realize the identical sloping angle by satisfying the phase-matching condition: [38,39]

$$G_1 = k_{spp} + k_{x,\theta}, \quad (1)$$

$$G_2 = k_{spp} - k_{x,\theta}. \quad (2)$$

Here, $G_{1,2} = 2\pi/P_{1,2}$ and $k_{x,\theta} = \sin\theta k_0$, where $k_0 = 2\pi/\lambda$ is the wavevector of the out-coupling light in free-space and θ is the angle of the emission. We would like to note that the above rigorous conditions for the realization of identical sloping angles for the outcoupled radiation can only approximately be satisfied (for small displacements and sloping angles) in our simplified design based on the usage of displaced circular ridges. In the following, we limit the considered displacements by 200 nm, a value that we estimated to be close to the crossover between the single- and double-beam outcoupling regimes for our configuration (see Supporting Information, section 1).

We perform the three-dimensional (3D) simulation for the proposed systems using the Finite-difference time-domain (FDTD) method. Figure 2a shows the schematic of the top view of the structure, which consists of 8 nanoridges with width w = 180 nm. When there is no displacement of the nanoridges in x direction, the structure would degenerate into normal bullseye rings with the default period P = 550 nm. The displacement in x direction is defined as $\Delta = (P_2 - P_1)/2$, where $P_2 + P_1 = 2P$. An electric dipole at wavelength $\lambda_0 = 670$ nm, viewed as a QE, is vertically orientated on the top of the substrate with a 50 nm distance and situates in the center of the inner nanoridge with

the radius of $r_0 = 520$ nm. The refractive index of HSQ is set as 1.41.[40] The permittivities of SiO_2 and Ag are taken from Ref. 41. Let us first check the near-field electric field distribution of the coupled systems in two different cross sections. Figure 2b presents the electric field distribution in the *y*-*z* plane (position indicated by the dashed line A in Figure 2a). It shows that a portion of the SPPs are scattered out of the plane when meet the inner gratings, while the rest part continues propagating along the surface until being converted into photons by outer gratings or decayed by the metal loss. It demonstrates that the symmetrically distributed rings in *y* direction convert the SPPs into outcoming photons with a symmetric shape. While for asymmetric Doppler gratings along the *x* direction with displacement $\Delta = 0.2$ μm, the SPPs are scattered and converted into photons unidirectionally in the *x*-*z* plane (position indicated by the dashed line B in Figure 2a). In the far-field pattern shown in Figure 2d, it is clearer that the outcoming photons in free space assembles a collimated bright spot in an off-axis direction, with the divergence angle of only ≅3°, as determined at the full-width-at-half-maximum (FWHM) of intensity distribution. The sloping unidirectional angle of the spot with respect to the center is 16.2°. The white circle indicates the view of the boundary of the NA 0.9 objective. The collection efficiency η_{ce}, defined as the ratio of the photon collected by the objective to the radiative emission from the quantum emitter[28], is 0.966, which is superior to most of the previously reported structures, such as nano-patch antennas[28] and Yagi-Uda antennas[31-33]. We would like to note that, although the horizontally excited QE can also realize the similar direction emission (the results are not presented here), the decay rate of the QE is several times lower than the vertical regime shown here.

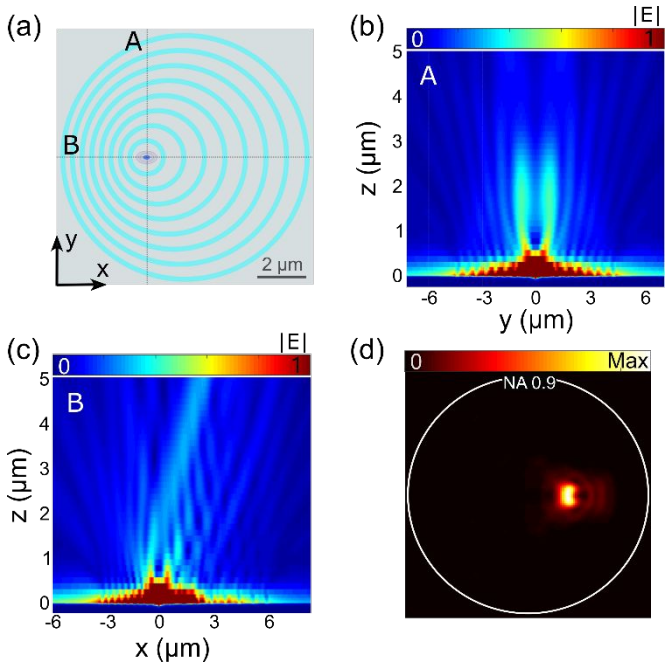

Figure 2. (a) The top view of the proposed coupled systems, consisting of 8 nanoridges with a vertical QE in the center. (b) The electric field distribution in the *y*-*z* plane. The cross section is cut along the dashed line A in Figure 2a. (c) The electric field distribution in the *x*-*z* plane. The cross-section is cut along the dashed line B in Figure 2a. (d) The simulation results of the far-field emission pattern. The white circle indicates the collective angle of the objective with NA = 0.9.

To experimentally demonstrate the unidirectional and off-axis emission, we fabricated the proposed systems with ~ 100-nm-diameter NDs, containing on average ~ 400 NV centers per ND (Adamas Nanotechnologies). These NDs can easily be located with the dark-field images, which makes it possible to preciously fabricate nanoridges around them (see Supporting Information). The substrate is fabricated by thermal evaporation of 3 nm Ti and 200 nm Ag on a Si wafer. Then, a 20-nm-thick SiO_2 layer is deposited through RF-sputtering. NDs are spin coated on the surface after the gold aligning markers being fabricated with standard electron-beam lithography (EBL). The relative position of a selected ND with respect to prefabricated gold aligning markers is determined using the

corresponding dark-field microscopy image. The HSQ circular nanoridges with different position displacement $\Delta = 0, 0.05, 0.1, 0.15,$ and 0.2 μm are subsequently fabricated around the selected NDs with the second EBL (see Supporting Information for fabrication details). As shown in Figure 3a-e, the selected NDs are situated in the center of the nanoridges, validating the accuracy in positioning. The NDs containing many NV centers would have many dipole momentums with random directions. To excite the vertically-oriented dipole, we use a tightly-focused radially-polarized 10-μW-pump cw-laser beam at the wavelength of 532 nm which produces a strong longitudinal electric field component at the focal plane. In particular, this optical pump configuration ensures that the excited NV centers (in the selected NDs) have sufficiently large projections of their radiative dipole transitions in the direction perpendicular to the surface, making thereby the experimental conditions similar to those used in our simulations (Figure 2). Upon excitation, the NDs decay to the SPPs on the dielectric-metal interface and then converted into the free-space emission by HSQ nanoridges (Figure 3f-j). The emission patterns with different structures are then taken from Fourier plane, as shown in Figure 3f-j. The white line indicates the collection boundary of the objective NA = 0.9. Figure 3a,f show a specific case that the structure is in azimuthal symmetry, where a doughnut-shape emission pattern is achieved in the far field. When the displacement is increased, the emission patterns could maintain concentrated spots, which is attributed to the azimuthal distribution of the rings. Moreover, the spot gradually shifts to aside with different unidirectional angles, demonstrating the tunability of the unidirectional emission. For the configuration with ridge displacement of $\Delta = 0.2$ μm in Figure 3e, the experimental measured angle of the collimated the spot is 17.3°, and the emission pattern coincides well with the simulation result shown in Figure 2d.

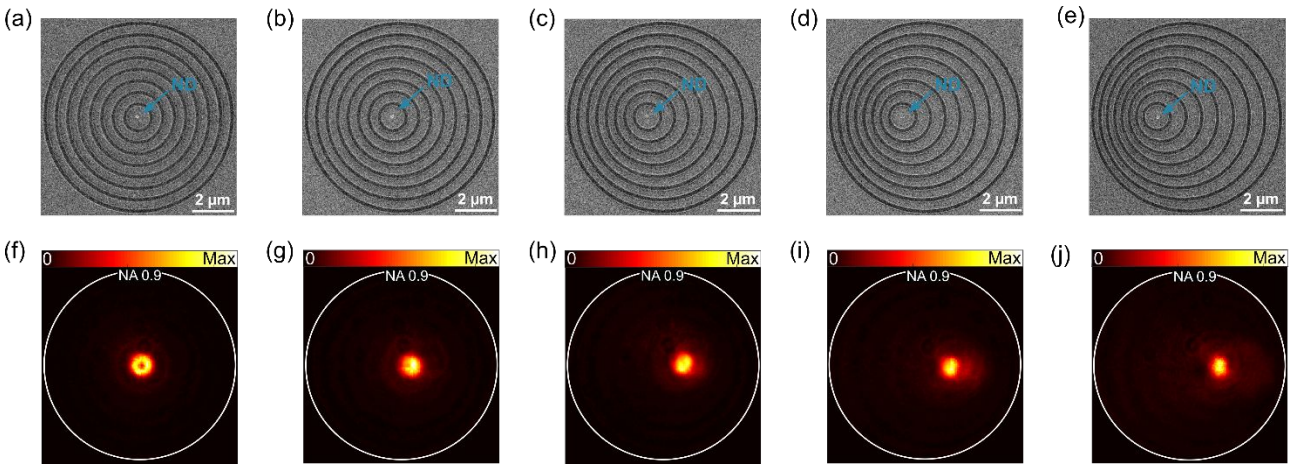

Figure 3. (a)-(e) The SEM images of the fabricated hybrid plasmonic-QE coupled systems with different ridge displacements $\Delta = 0, 0.05, 0.1, 0.15,$ and 0.2 μm in x direction, respectively. The NDs are situated in the center of the inner rings with the HSQ nanoridges being fabricated arround. (f)-(j) The corresponding Fourier plane images of the different samples. The while line indicates images are taken with an objective of NA = 0.9.

Figure 4a shows the spectra of the fabricated samples with different displacements. All of them have two small peaks around 575 nm and 637 nm, which are fingerprints for the neutral (NV^0) and negative charge state (NV^-).[42] The fluorescence of the NDs has a large photon distribution around 670 nm. For better correspondence with the simulation wavelength, we used a 676 ± 15nm band-passing filter to block light at other wavelengths, as well as the pump laser beam. Figure 4b presents the relationship between the ridge displacement and the outcoupling angle of the unidirectional emission. The experimental results for different Δ are in excellent agreement with the corresponding numerical simulations in the whole range of displacements (0 - 200 nm). The design outcoupling angles are consistent with both numerically simulated and experimentally measured values only for small displacements ($\leq$ 100 nm), while progressively overestimating the outcoupling angles for larger

displacements. As such, the discrepancy should be expected for large (> 100 nm) displacements due to approximations involved in the simplified design approach (based on displaced circular ridges) that results in two phase-matched outcoupling directions corresponding to the two different periods, P_1 and P_2 (see Supporting Information, section 1). The fact, that the deviation seems to better follow the smallest (of two) outcoupling angle, may be ascribed to stronger SPP scattering in the forward direction[43] that would enhance the contribution from the large period (P_2) grating, but other important factors might be involved (see Supporting Information, section 1). The collection efficiency as a function of the circular ridge displacement is also calculated. It shows that with different displacements the collection efficiencies keep around 0.965, which is promising for efficiently extracting photons out from nanoscale plasmonic-QEs coupled system. Therefore, the proposed coupled systems can act as a functional interconnect between the QEs and free-space complicated optical systems. Based on the design, in the future, it is possible to achieve more active and flexible manipulation of the direction of QE emission by introducing phase-change materials,[44,45] electrical gating,[46] and modulating surrounding environment[47] into the coupled system.

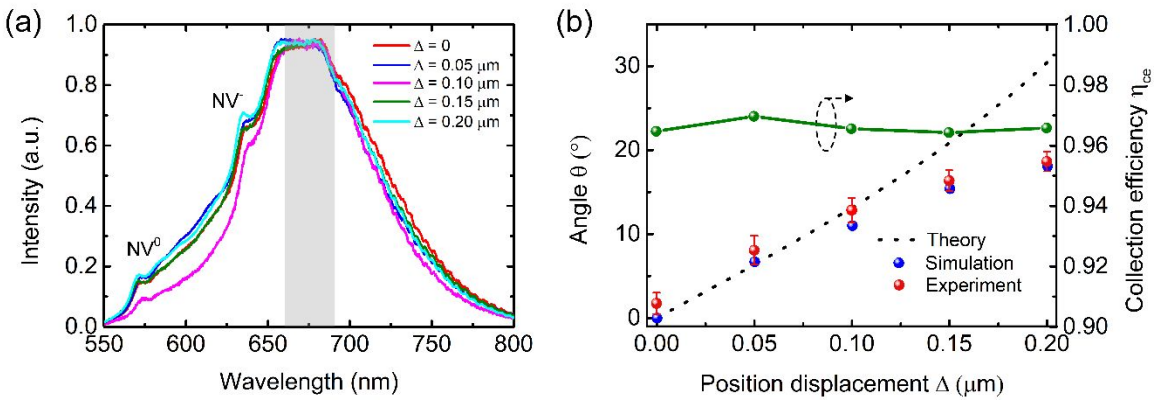

Figure 4. (a) The normalized spectra of the emission from the fabricated hybrid plasmonic-QEs coupled systems. The gray area indicates the range of band-passing filter (676 ± 15nm). (b) The

design, simulated, and experimental values of the outcoupling angle as a function of the circular ridge displacement. The green line shows the collection efficiency with a NA = 0.9 objective.

In summary, we have proposed hybrid plasmonic-QEs coupled systems consisting of bullseye-like Doppler nanoridges with NDs situated in the center of the inner rings. We experimentally demonstrated that the proposed systems have the capability of directing the emission from NVs to a unidirectional and off-axis collimated beam in the far field. It shows that the unidirectional angle can be as large as 17.3° with the circular ridge displacement of $\Delta = 0.2$ μm. The collection efficiency can maintain a high value about 0.965 with a collective objective of NA = 0.9. The off-axis angle is relevant to the position shift, demonstrating the ability of the proposed systems to actively guide the direction of the emission from QEs. This work paves the venue to flexibly connect the quantum emission with complex optical systems.

ASSOCIATED CONTENT

Supporting Information.

Section S1: Numerical simulation for determining the wavelengths of SPPs and the default period of gratings. Section S2: Detailed description of the fabrication of the samples. Section S3: Schematic of the experimental setup.

AUTHOR INFORMATION

Corresponding Author

*(C.Y.Z.) E-mail: changing.zhao@sjtu.edu.cn

*(S.I.B.) E-mail: seib@mci.sdu.dk

ACKNOWLEDGEMENTS

C.Y.Z. and Y.H.K. acknowledge the support from the National Natural Science Foundation of China (Grants No. 51636004) and the China Scholarship Council (No.201806230179). The authors gratefully acknowledge financial support from the European Research Council, Grant 341054 (PLAQNAP). S.I.B. acknowledges the support from the Villum Kann Rasmussen Foundation (Award in Technical and Natural Sciences 2019). F.D. acknowledges the supporting of Villum Experiment (Grant No. 00022988) from Villum Fonden. The authors thank Sebastian K. H. Andersen and Shailesh Kumar for helpful discussions.

Supporting Information

Supporting Information Available:

Qualitative analysis of our design approach; Numerical simulation to estimate the nanoridge period; Detailed sample fabrication description; Experimental setup used for characterization.

This material is available free of charge via the Internet at http://pubs.acs.org

REFERENCES

(1) O'Brien, J. L.; Furusawa, A.; Vučković, J. Photonic quantum technologies. *Nature Photon* **2009**, *3*, 687–695.

(2) Togan, E.; Chu, Y.; Trifonov, A. S.; Jiang, L.; Maze, J.; Childress, L.; Dutt, M. V. G.; Sørensen, A. S.; Hemmer, P. R.; Zibrov, A. S.; Lukin, M. D. Quantum entanglement between an optical photon and a solid-state spin qubit. *Nature* **2010**, *466*, 730−734.

(3) Bernien, H.; Hensen, B.; Pfaff, W.; Koolstra, G.; Blok, M. S.; Robledo, L.; Taminiau, T. H.; Markham, M.; Twitchen, D. J.; Childress, L.; Hanson, R. Heralded entanglement between solid-state qubits separated by three metres. *Nature* **2013**, *497*, 86−90.

(4) Kok, P.; Munro, W. J.; Nemoto, K.; Ralph, T. C.; Dowling, J. P.; Milburn, G. J. Linear optical quantum computing with photonic qubits. *Rev. Mod. Phys.* **2007**, *79*, 135−174.

(5) Gaita-Ariño, A.; Luis, F.; Hill, S.; Coronado, E. Molecular spins for quantum computation. *Nat. Chem.* **2019**, *11*, 301−309.

(6) Sushkov, A. O.; Chisholm, N.; Lovchinsky, I.; Kubo, M.; Lo, P. K.; Bennett, S. D.; Hunger, D.; Akimov, A.; Walsworth, R. L.; Park, H.; Lukin, M. D. All-optical sensing of a single-molecule electron spin. *Nano Lett.* **2014**, *14*, 6443−6448.

(7) Degen, C. L.; Reinhard, F.; Cappellaro, P. Quantum sensing. *Rev. Mod. Phys.* **2017**, *89*, 035002.

(8) Kongsuwan, N.; Xiong, X.; Bai, P.; You, J. B.; Png, C. E.; Wu, L.; Hess, O. Quantum plasmonic immunoassay sensing. *Nano Lett.* **2019**, *19* (9), 5853-5861.

(9) Hwang, J.; Pototschnig, M.; Lettow, R.; Zumofen, G.; Renna, A.; Götzinger, S.; Sandoghdar, V. A single-molecule optical transistor. *Nature* **2009**, *460*, 76−80.

(10) Maser, A.; Gmeiner, B.; Utikal, T.; Götzinger, S.; Sandoghdar, V. Few-photon coherent nonlinear optics with a single molecule. *Nat. Photonics* **2016**, *10*, 450.

(11) Michler, P.; Imamoglu, A.; Mason, M. D.; Carson, P. J.; Strouse, G. F.; Buratto, S. K. Quantum correlation among photons from a single quantum dot at room temperature. *Nature* **2000**, *406*, 968.

(12) Ates, S.; Ulrich, S. M.; Ulhaq, A.; Reitzenstein, S.; Löffler, A.; Hofling, S.; Forchel, A.; Michler, P. Non-resonant dot–cavity coupling and its potential for resonant single-quantum-dot spectroscopy. *Nat. Photonics* **2009**, *3*, 724.

(13) Abudayyeh, H.; Lubotzky, B.; Majumder, S.; Hollingsworth, J. A.; Rapaport, R. Purification of single photons by temporal heralding of quantum dot sources. *ACS Photonics* **2019**, *6* (2), 446-452.

(14) Beams, R.; Smith, D.; Johnson, T. W.; Oh, S.-H.; Novotny, L.; Vamivakas, A. N. Nanoscale fluorescence lifetime imaging of an optical antenna with a single diamond NV center. *Nano Lett.* **2013**, *13*, 3807−3811.

(15) Kumar, S.; Huck, A.; Andersen, U. L. Efficient coupling of a single diamond color center to propagating plasmonic gap modes. *Nano Lett.* **2013**, *13*, 1221−1225.

(16) Aharonovich, I.; Englund, D.; Toth, M. Solid-state single-photon emitters. *Nat. Photonics* **2016**, *10*, 631−641.

(17) Hadden, J. P.; Harrison, J. P.; Stanley-Clarke, A. C.; Marseglia, L.; Ho, Y.-L. D.; Patton, B. R.; O'Brien, J. L.; Rarity, J. G. Strongly enhanced photon collection from diamond defect centers under microfabricated integrated solid immersion lenses. *Appl. Phys. Lett.* **2010**, *97*, 241901.

(18) Marseglia, L.; Hadden, J.; Stanley-Clarke, A.; Harrison, J.; Patton, B.; Ho, Y.-L.; Naydenov, B.; Jelezko, F.; Meijer, J.; Dolan, P.; Smith, J.; Rarity, J.; O'Brien, J. Nanofabricated solid immersion lenses registered to single emitters in diamond. *Appl. Phys. Lett.* **2011**, *98*, 133107.

(19) Schröder, T.; Gadeke, F.; Banholzer, M. J.; Benson, O. Ultrabright and efficient single-photon generation based on nitrogen-vacancy centres in nanodiamonds on a solid immersion lens. *New J. Phys.* **2011**, *13*, 055017.

(20) Fernandez-Domínguez, A. I.; Bozhevolnyi, S. I.; Mortensen, N. A. Plasmon-enhanced generation of nonclassical light. *ACS Photonics* **2018**, *5*, 3447−3451.

(21) Li, L.; Chen, E. H.; Zheng, J.; Mouradian, S. L.; Dolde, F.; Schrö der, T.; Karaveli, S.; Markham, M. L.; Twitchen, D. J.; Englund, D. Efficient photon collection from a nitrogen vacancy center in a circular bullseye grating. *Nano Lett.* **2015**, *15*, 1493−1497.

(22) Andersen, S. K. H.; Bogdanov, S.; Makarova, O.; Xuan, Y.; Shalaginov, M. Y.; Boltasseva, A.; Bozhevolnyi, S. I.; Shalaev, V. M. Hybrid plasmonic bullseye antennas for efficient photon collection. *ACS Photonics* **2018**, *5* (3), 692.

(23) Benedikter, J.; Kaupp, H.; Hümmer, T.; Liang, Y.; Bommer, A.; Becher, C.; Krueger, A.; Smith, J. M.; Hansch, T. W.; Hunger, D. Cavity-Enhanced Single-Photon Source Based on the Silicon-Vacancy Center in Diamond. *Phys. Rev. Appl.* **2017**, *7* (2), 024031.

(24) Koenderink, A. F. Single-photon nanoantennas. *ACS Photonics* **2017**, *4*, 710−722.

(25) Hugall, J. T.; Singh, A.; van Hulst, N. F. Plasmonic Cavity Coupling. *ACS Photonics* **2018**, *5*, 43−53.

(26) Bozhevolnyi, S. I.; Khurgin, J. Fundamental limitations in spontaneous emission rate of single-photon sources. *Optica* **2016**, *3*, 1418−1421.

(27) Chikkaraddy, R.; de Nijs, B.; Benz, F.; Barrow, S. J.; Scherman, O. A.; Rosta, E.; Demetriadou, A.; Fox, P.; Hess, O.; Baumberg, J. J. Single-molecule strong coupling at room temperature in plasmonic nanocavities. *Nature* **2016**, *535*, 127−130.

(28) Akselrod, G. M.; Argyropoulos, C.; Hoang, T. B.; Ciracì, C.; Fang, C.; Huang, J.; Smith, D. R.; Mikkelsen, M. H. Probing the mechanisms of large Purcell enhancement in plasmonic nanoantennas. *Nat. Photonics* **2014**, *8*, 835−840.

(29) Hoang, T. B.; Akselrod, G. M.; Mikkelsen, M. H. Ultrafast room-temperature single photon emission from quantum dots coupled to plasmonic nanocavities. *Nano Lett.* **2016**, *16*, 270−275.

(30) Curto, A. G.; Volpe, G.; Taminiau, T. H.; Kreuzer, M. P.; Quidant, R.; van Hulst, N. F. Unidirectional emission of a quantum dot coupled to a nanoantenna. *Science* **2010**, *329*, 930.

(31) Kosako, T.; Kadoya, Y.; Hofmann, H. F. Directional Control of Light by a Nano-Optical Yagi-Uda Antenna. *Nat. Photonics* **2010**, *4*, 312−315.

(32) Ramezani, N.; Casadei, A.; Grzela, G.; Matteini, F.; Tütüncüoglu, G.; Rüffer, D.; Fontcuberta I Morral, A.; Gomez Rivas, J. Hybrid semiconductor nanowire–metallic Yagi-Uda antennas. *Nano Lett.* **2015**, *15*, 4889−4895.

(33) Ho, J.; Fu, Y. H.; Dong, Z.; Paniagua-Dominguez, R.; Koay, E. H. H.; Yu, Y. F.; Valuckas, V.; Kuznetsov, A. I.; Yang, J. K. W. Highly directive hybrid metal–dielectric Yagi-Uda nanoantennas. *ACS Nano* **2018**, *12* (8), 8616-8624.

(34) Choy, J. T.; Bulu, I.; Hausmann, B. J.; Janitz, E.; Huang, I.-C.; Lončar, M. Spontaneous emission and collection efficiency enhancement of single emitters in diamond via plasmonic cavities and gratings. *Appl. Phys. Lett.* **2013**, *103*, 161101.

(35) Livneh, N.; Harats, M. G.; Yochelis, S.; Paltiel, Y.; Rapaport, R. Efficient collection of light from colloidal quantum dots with a hybrid metal–dielectric nanoantenna. *ACS Photonics* **2015**, *2*, 1669 -1674.

(36) Livneh, N.; Harats, M. G.; Istrati, D.; Eisenberg, H. S.; Rapaport, R. Highly directional room-temperature single photon device. *Nano Lett.* **2016**, *16*, 2527−2532.

(37) Stella, U.; Boarino, L.; Leo, N. D.; Munzert, P.; Descrovi, E. Enhanced Directional Light Emission Assisted by Resonant Bloch Surface Waves in Circular Cavities. *ACS Photonics* **2019**, *6* (8), 2073-2082.

(38) Novotny, L.; Hecht, B. *Principles of Nano-Optics, 2nd ed.*; Cambridge University Press, 2012.

(39) Romanato, F.; Hong, L. K.; Kang, H. K.; Wong, C. C.; Yun, Z.; Knoll, W. Azimuthal dispersion and energy mode condensation of grating-coupled surface plasmon polaritons. *Phys. Rev. B* **2008**, *77*, 245435.

(40) Siampour, H.; Kumar, S.; Bozhevolnyi, S. I. Nanofabrication of plasmonic circuits containing single photon sources. *ACS Photonics* **2017**, *4*, 1879−1884.

(41) Palik, E. D. *Handbook of optical constants of solids*; Academic Press, 1998.

(42) Andersen, S. K. H.; Kumar, S.; Bozhevolnyi, S. I. Ultrabright linearly polarized photon generation from a nitrogen vacancy center in a nanocube dimer antenna. *Nano Lett.* **2017**, *17*, 3889−3895.

(43) Evlyukhin, A. B.; Bozhevolnyi, S. I. Point-dipole approximation for surface plasmon polariton scattering: Implications and limitations. *Phys. Rev. B* **2005**, *71*, 134304.

(44) Shaltout, A. M.; Shalaev, V. M.; Brongersma, M. L. Spatiotemporal light control with active metasurfaces. *Science* **2019**, *364*, No. eaat3100.

(45) Wang, Q.; Rogers, E. T.; Gholipour, B.; Wang, C.-M.; Yuan, G.; Teng, J.; Zheludev, N. I. Optically reconfigurable metasurfaces and photonic devices based on phase change materials. *Nat. Photonics* **2016**, *10* (1), 60.

(46) Park, J.; Kang, J.; Kim, S.; Liu, X.; Brongersma, M. Dynamic Reflection Phase and Polarization Control in Metasurfaces. *Nano Lett.* **2017**, *17*, 407−413.

(47) Komar, A.; Paniagua-Domínguez, R.; Miroshnichenko, A.; Yu, Y. F.; Kivshar, Y. S.; Kuznetsov, A. I.; Neshev, D. Dynamic beam switching by liquid crystal tunable dielectric metasurfaces. *ACS Photonics* **2018**, *5*, 1742−1748.

For Table of Contents Use Only

Directional off-normal photon streaming from hybrid plasmon-emitter coupled metasurfaces

Yinhui Kan, Fei Ding, Changying Zhao, Sergey I. Bozhevolnyi

A novel approach to directional off-normal photon steaming from hybrid plasmon-emitter coupled metasurfaces is described. It entails phase matching of QE-excited circularly diverging surface plasmons to a well-collimated off-normal propagating photon stream by using circular nanoridges with displaced centers. Fabrication characterization of the metasurface consisting of dielectric circular nanoridges with displacement fabricated on a silver around the QEs are reported.